ACS central science

Research Article

http://pubs.acs.org/journal/acscii

Highly Active Fe Sites in Ultrathin Pyrrhotite Fe_7S_8 Nanosheets Realizing Efficient Electrocatalytic Oxygen Evolution

Shichuan Chen,[†] Zhixiong Kang,[†] Xiaodong Zhang,[*,†] Junfeng Xie,[‡] Hui Wang,[†] Wei Shao,[†] XuSheng Zheng,[§] Wensheng Yan,[§] Bicai Pan,[†] and Yi Xie[*,†]

[†]Hefei National Laboratory for Physical Science at the Microscale, CAS Center for Excellence in Nanoscience, Collaborative Innovation Center of Chemistry for Energy Materials, University of Science and Technology of China, Hefei, 230026, P. R. China

[‡]College of Chemistry, Chemical Engineering and Materials Science, Shandong Normal University, Jinan, 250014, P. R. China

[§]National Synchrotron Radiation Laboratory, University of Science and Technology of China, Hefei, 230029, P. R. China

Supporting Information

ABSTRACT: Identification of active sites in an electrocatalyst is essential for understanding of the mechanism of electrocatalytic water splitting. To be one of the most active oxygen evolution reaction catalysts in alkaline media, Ni–Fe based compounds have attracted tremendous attention, while the role of Ni and Fe sites played has still come under debate. Herein, by taking the pyrrhotite Fe_7S_8 nanosheets with mixed-valence states and metallic conductivity for examples, we illustrate that Fe could be a highly active site for electrocatalytic oxygen evolution. It is shown that the delocalized electrons in the ultrathin Fe_7S_8 nanosheets could facilitate electron transfer processes of the system, where d orbitals of Fe^{II} and Fe^{III} would be overlapped with each other during the catalytic reactions, rendering the ultrathin Fe_7S_8 nanosheets to be the most efficient Fe-based electrocatalyst for water oxidation. As expected, the ultrathin Fe_7S_8 nanosheets exhibit promising electrocatalytic oxygen evolution activities, with a low overpotential of 0.27 V and a large current density of 300 mA cm^{-2} at 0.5 V. This work provides solid evidence that Fe could be an efficient active site for electrocatalytic water splitting.

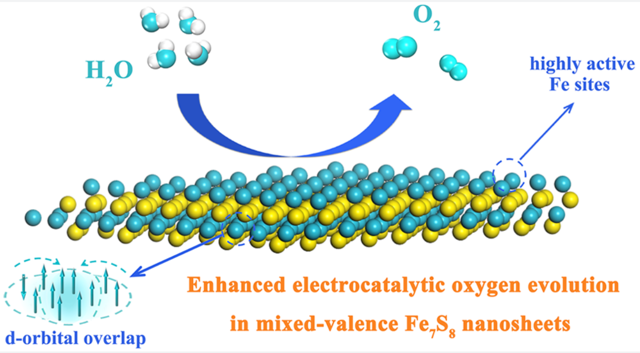

INTRODUCTION

Electrochemical water splitting was regarded as a promising method for clean and sustainable energy conversion and storage, where the oxygen evolution reaction (OER) is the bottleneck in water splitting owing to its complex four-electron redox process with slow kinetics.[1−5] Generally speaking, a catalyst must be applied during the OER processes to overcome the high overpotential and promote the reaction rate of water electrolysis. Currently, the most efficient OER electrocatalysts are noble metal based catalysts such as IrO_2 and RuO_2, while their scarcity and high cost greatly hamper large-scale applications.[6,7] For these reasons, extensive efforts have been undertaken to develop highly active, durable, and low-cost alternatives, such as the earth-abundant transition-metal-based (Ni, Co, Fe, Mn, etc.) compounds.[8−16]

A review of the pioneering study suggests Ni–Fe electrocatalysts to be the most active OER catalysts in alkaline media, which show significantly enhanced catalytic activity compared to that reported for either Ni- or Fe-based electrocatalyst alone, and even surpass some of the noble metal based catalysts.[11,17−21] For example, Lu et al. showed that the overpotential of electrodeposited Ni–Fe hydroxide nanosheets at 10 mA cm^{-2} could be as low as 215 mV,[22] while that for Ni- or Fe-based electrocatalysts is usually in the range of 350–450 mV and 500 mV, respectively.[19,23] In addition, the OER activity of Ni–Fe oxide thin film with 40% Fe atom is about 3 orders and 2 orders of magnitude higher than that of the deposited Fe film and Ni film, respectively.[11] Although great successes have been achieved in the design of highly active Ni–Fe electrocatalysts, the role of Ni and Fe sites played in the outstanding catalytic activity was under debate, and it is still uncertain which one is the actual catalytic active site.[24−28] Because the Ni-based compounds generally possess higher OER activity than Fe-based samples, Ni was usually assumed to be the reactive site for water oxidation in Ni–Fe electrocatalysts.[29−31] For instance, a series of studies implied that Fe^{III} in Ni–Fe catalysts promotes the formation of Ni^{IV} during the electrocatalytic reactions, which was assumed to be the active site during the OER process.[18,32,33] Moreover, the work of Louie et al. showed that Ni sites in the electrodeposited Ni–Fe film contain a structural unit similar to NiOOH, conjecturing that Ni centers serve as active sites for OER.[11]

Received: September 11, 2017
Published: October 24, 2017

DOI: 10.1021/acscentsci.7b00424
ACS Cent. Sci. 2017, 3, 1221−1227

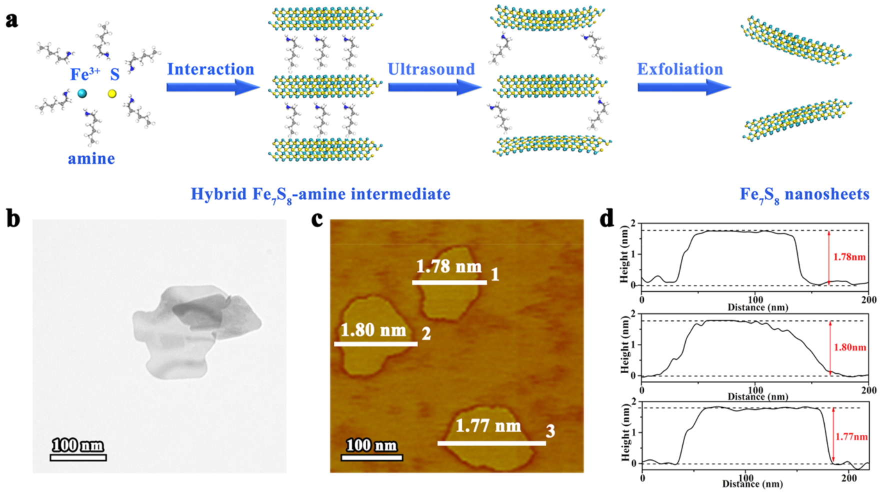

Figure 1. Synthesis and morphology study. (a) Schematic introduction for the formation of ultrathin Fe_7S_8 nanosheets. (b) TEM image of Fe_7S_8 nanosheets. (c, d) AFM image and corresponding height profiles of Fe_7S_8 nanosheets.

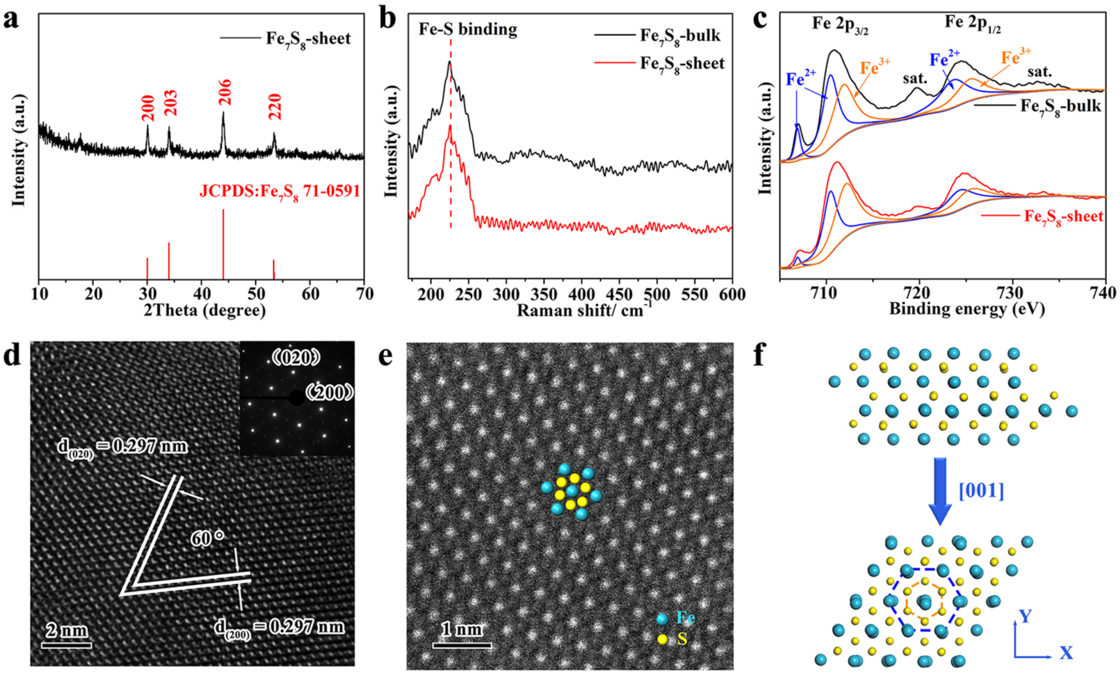

Figure 2. Structural characterizations. (a) XRD pattern of the recollected powder of nanosheets. (b) Raman spectra of the Fe_7S_8 nanosheets and bulk sample. (c) XPS Fe 2p spectra of Fe_7S_8 nanosheets and bulk sample. (d) HRTEM image and SAED pattern of typical Fe_7S_8 nanosheets. (e) Atomic-resolution HAADF-STEM image of Fe_7S_8 nanosheets. (f) Crystal structure of Fe_7S_8.

However, the latest spectroscopic and computational studies proposed that Fe is likely to be active site in Ni−Fe electrocatalysts too, especially for the detection of Fe^{IV} during OER processes.[34,35] Despite that numerous studies have shown that the incorporation of Fe into Ni-based compounds could dramatically enhance their catalytic activity, it is still hard to identify whether Fe would be the active site or not for the lack of efficient Fe-based OER electrocatalysts. So far, unary Fe-based electrocatalysts generally possess large overpotential and low current density in OER tests.[36,37] Thus, designing efficient electrocatalysts with highly active Fe sites is crucial for understanding the role of Fe played during the oxygen evolution processes, which may bring new vitality to the area of OER.

Inspired by the mixed-valence character of state-of-the-art Ni^{II}−Fe^{III} catalysts, we focused on the Fe-based electrocatalysts with mixed-valence states of Fe^{II} and Fe^{III}. Given that low electrical conductivity was usually accounted for the poor apparent OER activity of Fe-based catalysts, searching for Fe-based compound with high electrical conductivity would be better. Bearing these in mind, we paid our attention to the pyrrhotite Fe_7S_8 with NiAs-based hexagonal structure, which possesses both mixed-valence state and intrinsic metallic character.[38,39] From the point of view that the two-dimensional (2D) nanosheets with atomic thickness would fully expose the active sites at the surface, thus the ultrathin Fe_7S_8 nanosheets would be ideal platforms for studying the reactivity of Fe sites in OER processes. Herein, taking the ultrathin Fe_7S_8 nanosheets as an example, we studied the role of Fe played during

DOI: 10.1021/acscentsci.7b00424
ACS Cent. Sci. 2017, 3, 1221−1227

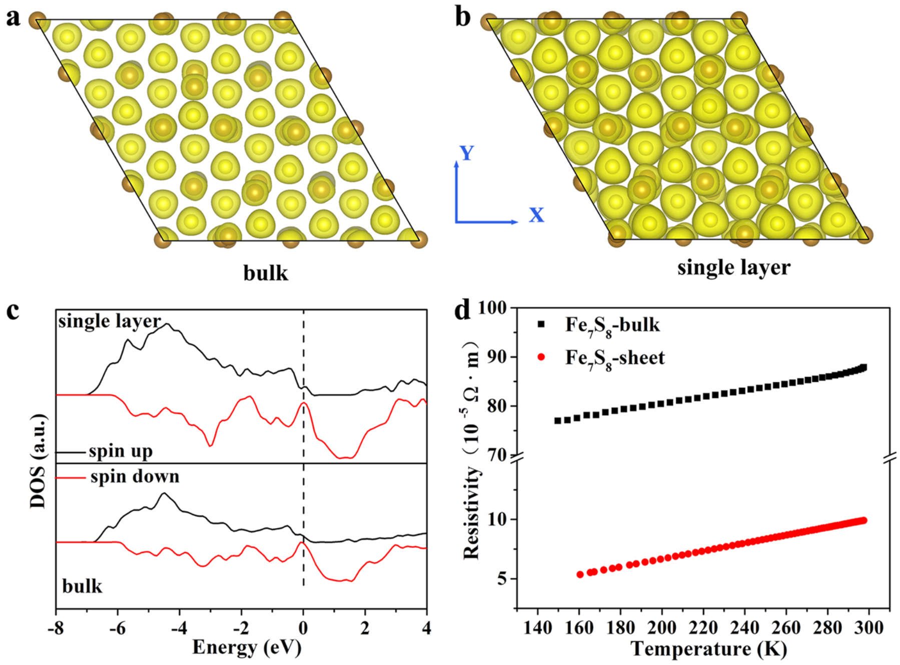

Figure 3. DFT calculations. (a, b) The charge-density wave of the bulk and single-layered Fe_7S_8, respectively. (c) Density of state (DOS) for the bulk and single-layered Fe_7S_8. (d) Comparison of temperature-dependent electrical resistivity of Fe_7S_8 nanosheets and bulk sample.

the oxygen evolution reactions, where the highly active Fe sites enable the ultrathin Fe_7S_8 nanosheets to be efficient catalysts for oxygen evolution. The identification of highly active Fe sites in OER processes would give new understanding on the mechanism of state-of-the-art Ni−Fe-based catalysts.

RESULTS AND DISCUSSION

Synthesis and Structural Characterizations. In this study, the ultrathin pyrrhotite Fe_7S_8 nanosheets with non-layered structure were successfully synthesized via a modified liquid exfoliation for the first time (Figure 1a). The amines with various lengths led to different interlamellar spacings of the inorganic−organic hybrid intermediate (Figure S4), indicating that the amines are vertically arranged in the lamellar structure. The morphology of as-exfoliated nanosheets was studied by transmission electron microscopy (TEM) image (Figure 1b), which shows a free-standing sheet-like transparency character, revealing their ultrathin thickness. Furthermore, the atomic force microscopy (AFM) technique was carried out to measure the thickness of as-exfoliated nanosheets. As shown in the AFM image and corresponding height profile (Figure 1c,d), the nanosheets show average thickness of about 1.78 nm, close to the thickness of a single-unit-cell Fe_7S_8 slab along the c axis.

The X-ray diffraction (XRD) pattern of the recollected powder of nanosheets (Figure 2a) could be readily indexed to the hexagonal phase of Fe_7S_8 with lattice constants of $a = 6.87$ Å, $c = 17.05$ Å (JCPDS Card No. 71-0591), and no peaks of any other phases can be detected. Moreover, the structure of as-obtained ultrathin Fe_7S_8 nanosheets was further studied by Raman spectra (Figure 2b), where the sharp peak at 220 cm^{-1} was assigned to the Fe−S binding of the hexagonal Fe_7S_8, indicating that the exfoliated Fe_7S_8 nanosheets maintain the structure of corresponding bulk counterpart.[40] As shown in Figure 2c, the valence states of exfoliated nanosheets were studied by X-ray photoelectron spectroscopy (XPS), where the Fe 2p spectrum of the Fe_7S_8 nanosheets shows similar shifts to that of the bulk sample. In detail, the Fe 2p peaks were deconvoluted and divided into Fe^{2+} and Fe^{3+} states, where the peaks located at 706.7, 710.4, and 723.6 eV were attributed to the Fe^{2+} state, whereas peaks at 711.8 and 725.4 eV were ascribed to signals of the Fe^{3+} state.[41,42] It is obvious that the prepared nanosheets possess mixed-valence character of Fe^{2+} and Fe^{3+}. The broadening and weakening XPS peaks for the Fe_7S_8 nanosheets compared with the bulk counterpart could be attributed to their ultrathin character.

The high-resolution TEM (HRTEM) image and corresponding selective area electron diffraction (SAED) pattern of the nanosheets show continuous and ordered lattice fringes with the lattice spacing of 0.297 nm, which correspond to the structure of hexagonal Fe_7S_8 (Figure 2d). To further evaluate the structure of the ultrathin Fe_7S_8 nanosheets, high-angle annular dark-field STEM image (HAADF-STEM) measurement was carried out on a typical nanosheet to see its atomic arrangements.[43] As presented in atomic-resolution HAADF-STEM image (Figure 2e), the bright and less bright spots are arranged in a hexagonal configuration, which correspond to the two distinct atoms, namely, Fe and S (blue and yellow dots representing Fe and S atoms, respectively), coinciding with the structure of hexagonal Fe_7S_8 as illustrated in Figure 2f. The above results clearly show that the ultrathin Fe_7S_8 nanosheets with mixed-valence states were successfully prepared.

Density-Functional Theory Calculations. Given the energetic degeneracy between the Fe^{2+} and Fe^{3+} configurations, extra electrons are easily delocalized between the two Fe sites of Fe_7S_8, which could be enhanced in the ultrathin 2D structure. Thus, it would be interesting for us to study the electronic structure of the ultrathin Fe_7S_8 nanosheets via density functional theory (DFT) calculations. As shown in Figure 3a,b, charge density of single-layered Fe_7S_8 shows enhanced orbital hybridization between Fe and S compared to the bulk material, implying the increased electrons in the single layer.[44] The DFT calculations in Figure 3c imply the metallic behavior of Fe_7S_8, in which the density of states (DOS) resides across the Fermi level and the single layer, showing an increase

DOI: 10.1021/acscentsci.7b00424
ACS Cent. Sci. 2017, 3, 1221−1227

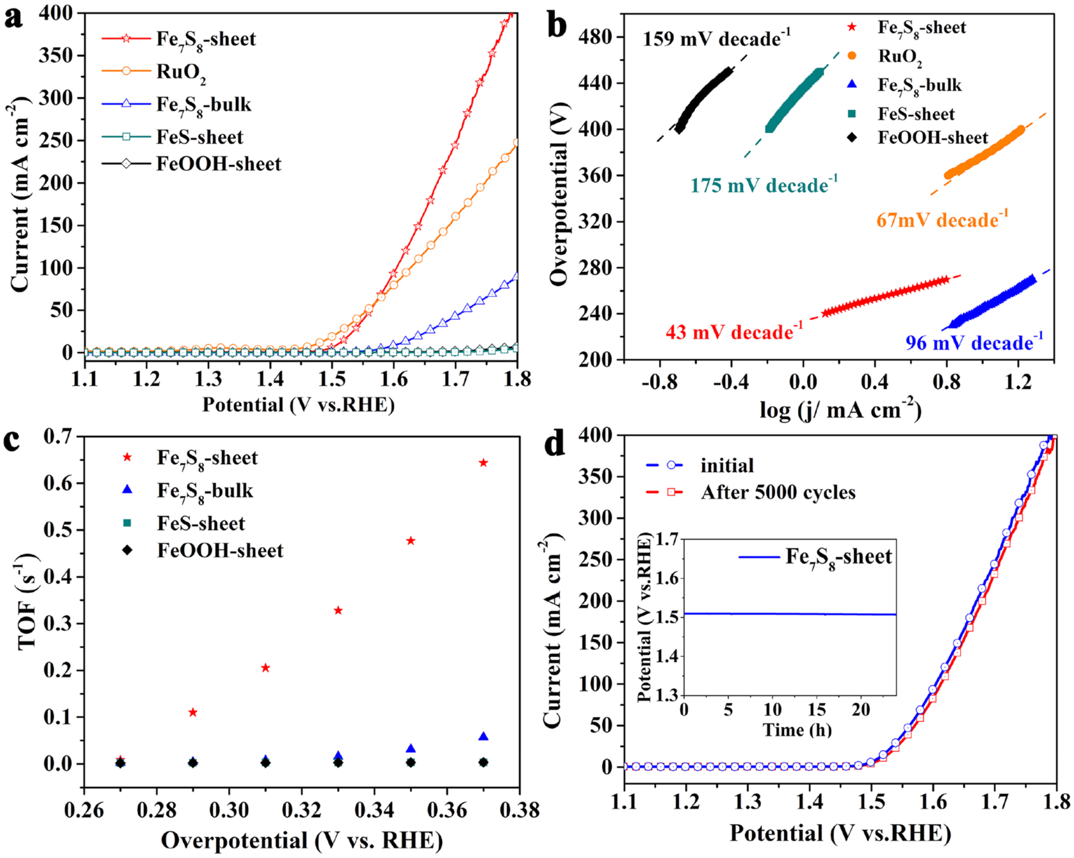

Figure 4. Electrochemical behaviors. (a) LSV curves of the tested samples. (b) Corresponding Tafel plots. (c) A plot of TOFs with respect to Fe atoms of Fe-based catalysts at different overpotentials. (d) LSV curves of the Fe_7S_8 nanosheets after 5000 CV cycles; inset is the chronopotentiometric curve obtained in 1 M KOH solution.

in DOS around the Fermi level compared to the bulk sample. The above results indicate that the single-layered Fe_7S_8 nanosheets would show enhanced conductivity with respect to their corresponding bulk counterparts. In order to confirm the electrical conductivity of the samples, temperature-dependent resistance tests were carried out (Figure 3d). As expected, resistivity of the Fe_7S_8 nanosheets takes on a slight increase with raised temperature, indicating an intrinsic metallic state of Fe_7S_8 nanosheets. Additionally, the value of resistivity for Fe_7S_8 nanosheets at room temperature (9.9×10^{-5} Ω·m) is about 8.8 times lower than that of the corresponding bulk counterpart, in agreement with the theoretical predictions. The intrinsic metallic character and superior electrical conductivity of the ultrathin Fe_7S_8 nanosheets render them to be efficient electrocatalysts for water oxidation.

It is well-known that the adsorption energy of H_2O molecules onto the active sites of catalyst plays a vital role in OER activity. In order to explore the potential application of Fe_7S_8 nanosheets in water oxidation, the DFT calculations were performed to study their H_2O absorption ability (Figure S8).[45,46] Specifically, the Fe_7S_8 nanosheets possess a more negative adsorption energy for H_2O molecules of about −1.29 eV, compared with that of Fe_7S_8-bulk (−0.52 eV) and FeS-sheets (−0.28 eV), implying that the Fe_7S_8 atomic layers would be an efficient electrocatalyst for water oxidation with highly active Fe sites.

OER Activity Measurements. To evaluate the electrocatalytic performances of as-obtained samples, the steady-state electrochemical measurements have been carried out in 1 M KOH solution using a typical three electrode cell setup (see details in the Supporting Information). Linear sweep voltammetry (LSV) curves in Figure 4a show that the Fe_7S_8 nanosheets display large electrocatalytic current density of 300 mA cm^{-2} at 0.5 V, which is much larger than that of Fe_7S_8 bulk (56.1 mA cm^{-2}, 5.38 times) and state-of-the-art RuO_2 electrocatalyst (185.2 mA cm^{-2}, 1.6 times), suggesting the Fe_7S_8 nanosheets to be excellent water oxidation catalysts. Moreover, the catalytic activity of the FeS sheets and FeOOH sheets with single-valence states were also carried out for comparison. Structural and morphology study of the FeS sheets and FeOOH sheets have been shown in Figure S2 and Figure S3. Detailedly, at 0.5 V, the current density of the FeOOH sheets and FeS sheets is only 1.54 mA cm^{-2} and 2.74 mA cm^{-2}, respectively, which values are much lower than those of both the Fe_7S_8 nanosheets and Fe_7S_8 bulk, implying that the Fe-based compounds with single-valence state have little activity for OER. Besides, only 0.27 V is required for the Fe_7S_8 nanosheets to reach a current density of 10 mA cm^{-2}, which is much smaller than that of all tested Fe-based samples and most previously reported OER catalysts (Tables S1 and S2), indicating their high electrocatalytic activity. Additionally, Tafel plots that reflect the OER increment rate of catalysts were carried out to examine their catalytic activity. A small Tafel slope is favorable for practical applications, because it will contribute to remarkably increased OER rate with an increase in overpotential. As seen from Figure 4b, the Fe_7S_8 nanosheet shows a smallest Tafel slope of 43 mV decade^{-1} among the tested samples, confirming the rapid kinetic information on

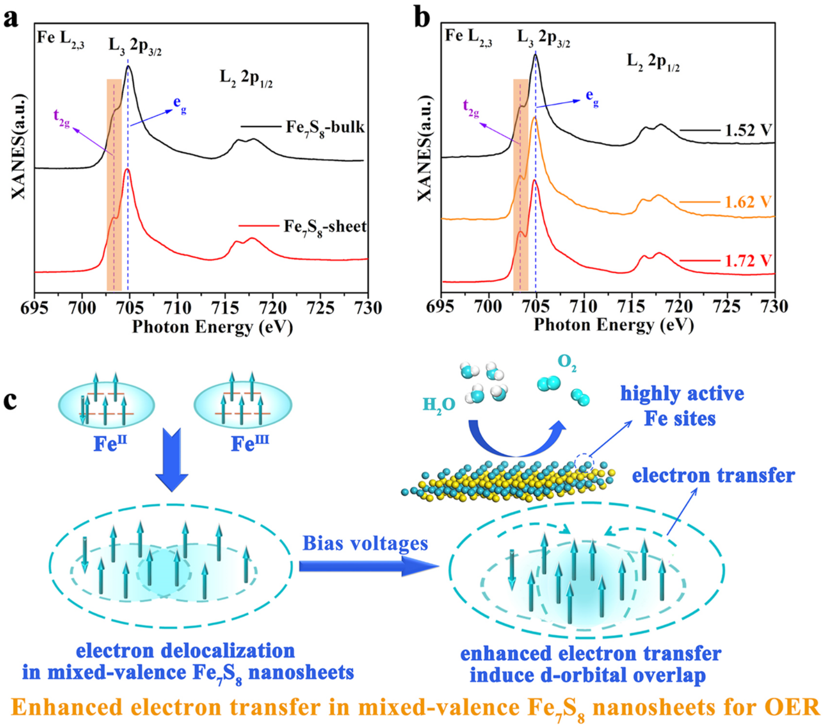

Figure 5. Spin states analyses. (a) XANES spectra of Fe_7S_8 nanosheets and bulk sample. (b) XANES spectra of Fe_7S_8 nanosheets collected at different bias voltages. (c) Schematic illustration for the formation of highly active Fe sites in the mixed-valence Fe_7S_8 nanosheets.

Fe_7S_8 nanosheets. It is obvious that the turnover frequency (TOF) of the Fe_7S_8 nanosheets is 0.34 s^{-1} at a quite small overpotential of 0.35 V, which is 20 times higher than that of bulk Fe_7S_8.

In order to further estimate the exposure of active sites, the electrochemically active surface areas (ECSAs) for the samples were estimated through the tested electrochemical double-layer capacitance (C_{dl}).[47] The C_{dl} value is proportional to ECSA and, thus, can reflect the density of ion-accessible sites of an electrocatalyst in the electrolyte. As displayed in Figure S7a, C_{dl} of Fe_7S_8 nanosheets is 3.8 times larger than that of the bulk sample, indicating the exposure of larger number of ion-accessible active sites in the nanosheets. Apart from the catalytic activity, electrical impedance spectroscopy (EIS) (Figure S7b) unravels a small charge-transfer resistance of the Fe_7S_8 nanosheets.

The long-term activity and durability is also a significant factor to evaluate an advanced electrocatalyst. As seen in Figure 4d, the activity of Fe_7S_8 nanosheets was nearly unchanged after 5000 CV cycles, indicating their high stability during the electrocatalytic reaction. The durability of Fe_7S_8 nanosheets can be further evaluated by chronopotentiometric measurements at $J = 10$ mA cm^{-2} for a long time. It is worth noting that ultrathin and mixed-valence characters would dramatically hamper the tendency of oxidation of the Fe_7S_8 nanosheets during the OER process for their rich surface dangling bonds and enhanced electron transfers, which render the nanosheets with exceptional stability.[36,48] All of the results above indicate Fe_7S_8 nanosheets to be excellent catalysts for oxygen evolution with highly active Fe sites.

Synchrotron-Based XANES Studies. Given the generally low electrocatalytic activity of the Fe-based compounds, it would be interesting for us to gain insights into the mechanism for the presence of highly active Fe sites in the mixed-valence Fe_7S_8 nanosheets. Bearing this in mind, synchrotron radiation-based X-ray absorption near edge structure (XANES), an effective technique to provide the spin orbital information on transition metal, was carried out to explore the electronic structure evolution of the Fe_7S_8 nanosheets during the OER tests.[49] As is known, the XANES spectra of Fe L_3 edge could be divided into two peaks that donated to be t_{2g} and e_g orbitals, respectively, whose intensity is a criterion to evaluate the total unoccupied states of the Fe 3d states.[50] As seen in Figure 5a, it is clear that the shoulder peak of t_{2g} is higher than that of Fe_7S_8 bulk (the shadowed part), indicating that the nanosheets possess a high density of t_{2g} unoccupied states, which may derive from their enhanced electron delocalization. Moreover, Fe L-edge XANES spectra of the Fe_7S_8 nanosheets in various OER stages, i.e., after electrochemical reaction at 1.52 V, 1.62 V, and 1.72 V (vs RHE) for 12 h, were further acquired to investigate the electronic structure of Fe atoms during the reactions. As seen from Figure 5b, the intensity of shoulder peak of t_{2g} in 703.2 eV was gradually increased with the increasing in reaction voltage, indicating that the t_{2g} unoccupied states are enhanced during the OER process. The phenomenon can be understood by the enhanced electron transfer in the ultrathin Fe_7S_8 nanosheets, where the d orbitals of Fe are overlapped with each other. As schematically illustrated in Figure 5c, owing to the delocalized electrons in the ultrathin nanosheets, the d orbitals of Fe^{II} and Fe^{III} show greater tendency to overlap with each other under external voltages, resulting in the enhanced t_{2g} unoccupied states of Fe. It is known that the enhanced unoccupied states indicate the loss of electrons in the system to some extent, where the metal atoms tend to be in high valence states. Although there is no obvious electron loss during the OER tests, the Fe sites in the ultrathin Fe_7S_8 nanosheets still represent the role of high valence played for the enhanced electron transfer between Fe^{II} and Fe^{III}, which should be the reason for their high reactivity.

■ CONCLUSIONS

In conclusion, we have proposed, for the first time, that an Fe-based compound with mixed-valence and metallic character could be an efficient electrocatalyst for oxygen evolution reaction by using the ultrathin pyrrhotite Fe_7S_8 nanosheets as examples. Both theoretical calculations and experiments show that the ultrathin Fe_7S_8 nanosheets possess enhanced electric conductivity and electron delocalization in comparison with the corresponding bulk sample. As directly revealed by the XANES spectra, the d orbitals of Fe^{II} and Fe^{III} in the ultrathin Fe_7S_8 nanosheets are intent to overlap with each other for the enhanced electron transfer process, resulting in the highly catalytic activity of Fe sites. Thus, the Fe_7S_8 nanosheets display improved OER catalytic activity compared with Fe_7S_8 bulk, FeS nanosheets, and FeOOH nanosheets, which manifest a small overpotential of 0.27 V and a large current density of 300 mA cm^{-2} at 0.5 V, to be the most reactive OER catalysts in Fe-based compounds. This work not only gives deep understanding on the role of Fe played in the OER process but also paves a practical way for the design of efficient electrocatalysts.

■ ASSOCIATED CONTENT

Ⓢ Supporting Information

The Supporting Information is available free of charge on the ACS Publications website at DOI: 10.1021/acscentsci.7b00424.

Experimental details, characterizations, and electrochemical properties study (PDF)

■ AUTHOR INFORMATION

Corresponding Authors

*E-mail: zhxid@ustc.edu.cn.
*E-mail: yxie@ustc.edu.cn.

ORCID

Xiaodong Zhang: 0000-0002-8288-035X
Yi Xie: 0000-0002-1416-5557

Notes

The authors declare no competing financial interest.

■ ACKNOWLEDGMENTS

The work was supported by National Key R&D Program of China (2017YFA0303500, 2017YFA0207301), the National Basic Research Program of China (2015CB932302), National Natural Science Foundation of China (U1532265, U1632149, 21401181, 21331005, 11621063), the Youth Innovation Promotion Association of CAS (2017493), Fundamental Research Funds for the Central University (WK2060190084), and the Key Research Program of Frontier Sciences (QYZDY-SSW-SLH011).

■ REFERENCES

(1) Suntivich, J.; May, K. J.; Gasteiger, H. A.; Goodenough, J. B.; Shao-Horn, Y. A perovskite oxide optimized for oxygen evolution catalysis from molecular orbital principles. *Science* **2011**, *334*, 1383−1385.

(2) Tarascon, J. M.; Armand, M. Issues and challenges facing rechargeable lithium batteries. *Nature* **2001**, *414*, 359−367.

(3) Mirzakulova, E.; Khatmullin, R.; Walpita, J.; Corrigan, T.; Vargas-Barbosa, N. M.; Vyas, S.; Oottikkal, S.; Manzer, S. F.; Hadad, C. M.; Glusac, K. D. Electrode-assisted catalytic water oxidation by a flavin derivative. *Nat. Chem.* **2012**, *4*, 794−801.

(4) Lee, S. W.; Carlton, C.; Risch, M.; Surendranath, Y.; Chen, S.; Furutsuki, S.; Yamada, A.; Nocera, D. G.; Shao-Horn, Y. The Nature of Lithium Battery Materials under Oxygen Evolution Reaction Conditions. *J. Am. Chem. Soc.* **2012**, *134*, 16959−16962.

(5) Xie, J.; Xie, Y. Transition Metal Nitrides for Electrocatalytic Energy Conversion: Opportunities and Challenges. *Chem. - Eur. J.* **2016**, *22*, 3588−3598.

(6) Fang, Y. H.; Liu, Z. P. Mechanism and Tafel Lines of Electro-Oxidation of Water to Oxygen on $RuO_2(110)$. *J. Am. Chem. Soc.* **2010**, *132*, 18214−18222.

(7) Lee, Y.; Suntivich, J.; May, K. J.; Perry, E. E.; Shao-Horn, Y. Synthesis and Activities of Rutile IrO_2 and RuO_2 Nanoparticles for Oxygen Evolution in Acid and Alkaline Solutions. *J. Phys. Chem. Lett.* **2012**, *3*, 399−404.

(8) Subbaraman, R.; Tripkovic, D.; Chang, K. C.; Strmcnik, D.; Paulikas, A. P.; Hirunsit, P.; Chan, M.; Greeley, J.; Stamenkovic, V.; Markovic, N. M. Trends in activity for the water electrolyser reactions on 3d M(Ni,Co,Fe,Mn) hydr(oxy)oxide catalysts. *Nat. Mater.* **2012**, *11*, 550−557.

(9) Feng, J. X.; Xu, H.; Dong, Y. T.; Ye, S. H.; Tong, Y. X.; Li, G. R. FeOOH/Co/FeOOH Hybrid Nanotube Arrays as High-Performance Electrocatalysts for the Oxygen Evolution Reaction. *Angew. Chem., Int. Ed.* **2016**, *55*, 3694−3698.

(10) Gao, M.; Sheng, W.; Zhuang, Z.; Fang, Q.; Gu, S.; Jiang, J.; Yan, Y. Efficient water oxidation using nanostructured alpha-nickel-hydroxide as an electrocatalyst. *J. Am. Chem. Soc.* **2014**, *136*, 7077−7084.

(11) Louie, M. W.; Bell, A. T. An investigation of thin-film Ni-Fe oxide catalysts for the electrochemical evolution of oxygen. *J. Am. Chem. Soc.* **2013**, *135*, 12329−12337.

(12) Chen, W.; Wang, H.; Li, Y.; Liu, Y.; Sun, J.; Lee, S.; Lee, J. S.; Cui, Y. In Situ Electrochemical Oxidation Tuning of Transition Metal Disulfides to Oxides for Enhanced Water Oxidation. *ACS Cent. Sci.* **2015**, *1*, 244−251.

(13) Chen, S.; Kang, Z.; Hu, X.; Zhang, X.; Wang, H.; Xie, J.; Zheng, X.; Yan, W.; Pan, B.; Xie, Y. Delocalized Spin States in 2D Atomic Layers Realizing Enhanced Electrocatalytic Oxygen Evolution. *Adv. Mater.* **2017**, *29*, 1701687.

(14) Zhou, S.; Miao, X.; Zhao, X.; Ma, C.; Qiu, Y.; Hu, Z.; Zhao, J.; Shi, L.; Zeng, J. Engineering electrocatalytic activity in nanosized perovskite cobaltite through surface spin-state transition. *Nat. Commun.* **2016**, *7*, 11510.

(15) Xie, J.; Zhang, X.; Zhang, H.; Zhang, J.; Li, S.; Wang, R.; Pan, B.; Xie, Y. Intralayered Ostwald Ripening to Ultrathin Nanomesh Catalyst with Robust Oxygen-Evolving Performance. *Adv. Mater.* **2017**, *29*, 1604765.

(16) Fang, Z.; Peng, L.; Lv, H.; Zhu, Y.; Yan, C.; Wang, S.; Kalyani, P.; Wu, X.; Yu, G. Metallic Transition Metal Selenide Holey Nanosheets for Efficient Oxygen Evolution Electrocatalysis. *ACS Nano* **2017**, *11*, 9550−9557.

(17) Xu, X.; Song, F.; Hu, X. A nickel iron diselenide-derived efficient oxygen-evolution catalyst. *Nat. Commun.* **2016**, *7*, 12324.

(18) Gong, M.; Li, Y.; Wang, H.; Liang, Y.; Wu, J. Z.; Zhou, J.; Wang, J.; Regier, T.; Wei, F.; Dai, H. An Advanced Ni−Fe Layered Double Hydroxide Electrocatalyst for Water Oxidation. *J. Am. Chem. Soc.* **2013**, *135*, 8452−8455.

(19) Lyons, M. E. G.; Brandon, M. P. The oxygen evolution reaction on passive oxide covered transition metal electrodes in alkaline solution. Part III-iron. *Int. J. Electrochem. Soc.* **2008**, *3*, 1463−1503.

(20) Gorlin, M.; Ferreira de Araujo, J.; Schmies, H.; Bernsmeier, D.; Dresp, S.; Gliech, M.; Jusys, Z.; Chernev, P.; Kraehnert, R.; Dau, H. Tracking Catalyst Redox States and Reaction Dynamics in Ni-Fe Oxyhydroxide Oxygen Evolution Reaction Electrocatalysts: The Role of Catalyst Support and Electrolyte pH. *J. Am. Chem. Soc.* **2017**, *139*, 2070−2082.

(21) Gorlin, M.; Chernev, P.; Ferreira de Araujo, J.; Reier, T.; Dresp, S.; Paul, B.; Krahnert, R.; Dau, H.; Strasser, P. Oxygen Evolution

Reaction Dynamics, Faradaic Charge Efficiency, and the Active Metal Redox States of Ni-Fe Oxide Water Splitting Electrocatalysts. *J. Am. Chem. Soc.* **2016**, *138*, 5603−5614.

(22) Lu, X.; Zhao, C. Electrodeposition of hierarchically structured three-dimensional nickel-iron electrodes for efficient oxygen evolution at high current densities. *Nat. Commun.* **2015**, *6*, 6616.

(23) Lyons, M. E.; Brandon, M. P. Redox switching and oxygen evolution electrocatalysis in polymeric iron oxyhydroxide films. *Phys. Chem. Chem. Phys.* **2009**, *11*, 2203−2217.

(24) Kim, S. H.; Tryk, D. A.; Antonio, M. R.; Carr, R.; Scherson, D. In-Situ X-Ray-Absorption Fine-Structure Studies of Foreign Metal-Ions in Nickel Hydrous Oxide Electrodes in Alkaline Electrolytes. *J. Phys. Chem.* **1994**, *98*, 10269−10276.

(25) Corrigan, D. A.; Conell, R. S.; Fierro, C. A.; Scherson, D. A. Insitu Mossbauer Study of Redox Processes in a Composite Hydroxide of Iron and Nickel. *J. Phys. Chem.* **1987**, *91*, 5009−5011.

(26) Trotochaud, L.; Ranney, J. K.; Williams, K. N.; Boettcher, S. W. Solution-cast metal oxide thin film electrocatalysts for oxygen evolution. *J. Am. Chem. Soc.* **2012**, *134*, 17253−17261.

(27) Ahn, H. S.; Bard, A. J. Surface Interrogation Scanning Electrochemical Microscopy of $\mathrm{Ni}_{(1\text{-}x)}\mathrm{Fe}_{(x)}\mathrm{OOH}$ $(0 < x < 0.27)$ Oxygen Evolving Catalyst: Kinetics of the "fast" Iron Sites. *J. Am. Chem. Soc.* **2016**, *138*, 313−318.

(28) Stevens, M. B.; Trang, C. D. M.; Enman, L. J.; Deng, J.; Boettcher, S. W. Reactive Fe-Sites in Ni/Fe (Oxy)hydroxide Are Responsible for Exceptional Oxygen Electrocatalysis Activity. *J. Am. Chem. Soc.* **2017**, *139*, 11361−11364.

(29) Diaz-Morales, O.; Ferrus-Suspedra, D.; Koper, M. T. M. The importance of nickel oxyhydroxide deprotonation on its activity towards electrochemical water oxidation. *Chem. Sci.* **2016**, *7*, 2639−2645.

(30) Trotochaud, L.; Young, S. L.; Ranney, J. K.; Boettcher, S. W. Nickel-iron oxyhydroxide oxygen-evolution electrocatalysts: the role of intentional and incidental iron incorporation. *J. Am. Chem. Soc.* **2014**, *136*, 6744−6753.

(31) Bediako, D. K.; Surendranath, Y.; Nocera, D. G. Mechanistic studies of the oxygen evolution reaction mediated by a nickel-borate thin film electrocatalyst. *J. Am. Chem. Soc.* **2013**, *135*, 3662−3674.

(32) Li, N.; Bediako, D. K.; Hadt, R. G.; Hayes, D.; Kempa, T. J.; von Cube, F.; Bell, D. C.; Chen, L. X.; Nocera, D. G. Influence of iron doping on tetravalent nickel content in catalytic oxygen evolving films. *Proc. Natl. Acad. Sci. U. S. A.* **2017**, *114*, 1486−1491.

(33) Taibi, M.; Ammar, S.; Schoenstein, F.; Jouini, N.; Fiévet, F.; Chauveau, T.; Greneche, J. M. Powder and film of nickel and iron-layered double hydroxide: Elaboration in polyol medium and characterization. *J. Phys. Chem. Solids* **2008**, *69*, 1052−1055.

(34) Chen, J. Y.; Dang, L.; Liang, H.; Bi, W.; Gerken, J. B.; Jin, S.; Alp, E. E.; Stahl, S. S. Operando Analysis of NiFe and Fe Oxyhydroxide Electrocatalysts for Water Oxidation: Detection of Fe(4)(+) by Mossbauer Spectroscopy. *J. Am. Chem. Soc.* **2015**, *137*, 15090−15093.

(35) Friebel, D.; Louie, M. W.; Bajdich, M.; Sanwald, K. E.; Cai, Y.; Wise, A. M.; Cheng, M. J.; Sokaras, D.; Weng, T. C.; Alonso-Mori, R. Identification of highly active Fe sites in (Ni,Fe)OOH for electro-catalytic water splitting. *J. Am. Chem. Soc.* **2015**, *137*, 1305−1313.

(36) Han, L.; Dong, S.; Wang, E. Transition-Metal (Co, Ni, and Fe)-Based Electrocatalysts for the Water Oxidation Reaction. *Adv. Mater.* **2016**, *28*, 9266−9291.

(37) Burke, M. S.; Zou, S.; Enman, L. J.; Kellon, J. E.; Gabor, C. A.; Pledger, E.; Boettcher, S. W. Revised Oxygen Evolution Reaction Activity Trends for First-Row Transition-Metal (Oxy)hydroxides in Alkaline Media. *J. Phys. Chem. Lett.* **2015**, *6*, 3737−3742.

(38) Becker, U.; Munz, A. W.; Lennie, A. R.; Thornton, G.; Vaughan, D. J. The atomic and electronic structure of the (001) surface of monoclinic pyrrhotite ($\mathrm{Fe}_7\mathrm{S}_8$) as studied using STM, LEED and quantum mechanical calculations. *Surf. Sci.* **1997**, *389*, 66−87.

(39) Shimada, K.; Mizokawa, T.; Mamiya, K.; Saitoh, T.; Fujimori, A.; Ono, K.; Kakizaki, A.; Ishii, T.; Shirai, M.; Kamimura, T. Spin-integrated and spin-resolved photoemission study of Fe chalcogenides. *Phys. Rev. B: Condens. Matter Mater. Phys.* **1998**, *57*, 8845−8853.

(40) El Mendili, Y.; Abdelouas, A.; El Hajj, H.; Bardeau, J. F. Phase transitions of iron sulphides formed by steel microbial corrosion. *RSC Adv.* **2013**, *3*, 26343.

(41) Zhang, K. L.; Zhang, T. W.; Liang, J. W.; Zhu, Y. C.; Lin, N.; Qian, Y. T. A potential pyrrhotite ($\mathrm{Fe}_7\mathrm{S}_8$) anode material for lithium storage. *RSC Adv.* **2015**, *5*, 14828−14831.

(42) Yamashita, T.; Hayes, P. Analysis of XPS spectra of Fe^{2+} and Fe^{3+} ions in oxide materials. *Appl. Surf. Sci.* **2008**, *254*, 2441−2449.

(43) Liu, Z.; Suenaga, K.; Wang, Z.; Shi, Z.; Okunishi, E.; Iijima, S. Identification of active atomic defects in a monolayered tungsten disulphide nanoribbon. *Nat. Commun.* **2011**, *2*, 213.

(44) Zhang, X.; Xu, J.; Wang, H.; Zhang, J.; Yan, H.; Pan, B.; Zhou, J.; Xie, Y. Ultrathin nanosheets of MAX phases with enhanced thermal and mechanical properties in polymeric compositions: $\mathrm{Ti}_3\mathrm{Si}_{(0.75)}\mathrm{Al}_{(0.25)}\mathrm{C}_2$. *Angew. Chem., Int. Ed.* **2013**, *52*, 4361−4365.

(45) Wu, G.; Li, N.; Zhou, D.-R.; Mitsuo, K.; Xu, B.-Q. Anodically electrodeposited Co+Ni mixed oxide electrode: preparation and electrocatalytic activity for oxygen evolution in alkaline media. *J. Solid State Chem.* **2004**, *177*, 3682−3692.

(46) Bao, J.; Zhang, X.; Fan, B.; Zhang, J.; Zhou, M.; Yang, W.; Hu, X.; Wang, H.; Pan, B.; Xie, Y. Ultrathin Spinel-Structured Nanosheets Rich in Oxygen Deficiencies for Enhanced Electrocatalytic Water Oxidation. *Angew. Chem., Int. Ed.* **2015**, *54*, 7399−7404.

(47) Song, F.; Hu, X. Exfoliation of layered double hydroxides for enhanced oxygen evolution catalysis. *Nat. Commun.* **2014**, *5*, 4477.

(48) Sun, Y.; Gao, S.; Xie, Y. Atomically-thick two-dimensional crystals: electronic structure regulation and energy device construction. *Chem. Soc. Rev.* **2014**, *43*, 530−546.

(49) Hocking, R. K.; Wasinger, E. C.; Yan, Y. L.; Degroot, F. M.; Walker, F. A.; Hodgson, K. O.; Hedman, B.; Solomon, E. I. Fe L-edge X-ray absorption spectroscopy of low-spin heme relative to non-heme Fe complexes: delocalization of Fe d-electrons into the porphyrin ligand. *J. Am. Chem. Soc.* **2007**, *129*, 113−125.

(50) Bashir, A.; Ikram, M.; Kumar, R.; Thakur, P.; Chae, K. H.; Choi, W. K.; Reddy, V. R. Structural, magnetic and electronic structure studies of $\mathrm{NdFe}_{(1\text{-}x)}\mathrm{Ni}_{(x)}\mathrm{O}_{(3)}$ (0 < /= x < /= 0.3). *J. Phys.: Condens. Matter* **2009**, *21*, 325501.